Influence of the coating resistivity on beam dynamics

A. Gamelin* and W. Foosang

Synchrotron SOLEIL, L'Orme des Merisiers, 91190 Saint-Aubin, France

(Received 9 January 2023; accepted 3 May 2023; published 19 May 2023)

Metallic coatings on the inner surfaces of the vacuum chambers are widely used in accelerators but the impact of the coating resistivity on the beam coupling impedance and beam dynamics is often not sufficiently evaluated. In this paper, it is shown that, for the usual coating thickness, the electrical resistivity of the coating can have a strong impact on the impedance and on the microwave instability threshold. In particular, using different nonevaporable getters coating as examples, the regime in which a coating with a lower resistivity produces a larger impedance than that with a higher resistivity is investigated.

DOI: 10.1103/PhysRevAccelBeams.26.054401

I. INTRODUCTION

Present and future accelerators often need to rely on metallic coating vast portions of their beam pipes to improve their performance or to reach their design goals. Nonevaporable getters (NEG) coatings are widely used to reach ultrahigh vacuum thanks to its distributed pumping properties [1–3]. Titanium nitride and amorphous carbon coating can be used in linear or circular colliders because of their low secondary electron yield to mitigate the electron cloud effect [4]. This article aims to shed some light on the impact of such coatings on the beam dynamics, more precisely, it underlines the importance of the electrical resistivity of the coating materials, often a parameter of underestimated importance because of its relatively unknown value.

The resistive-wall impedance, which is produced by the beam chamber finite conductivity, and the subsequent collective effects are highly impacted by coatings. This impact is especially important for very large machines [5] or for machines with very small beam pipe dimensions such as some of the fourth generation light sources [6]. It has been demonstrated that there is a regime where the resistive-wall impedance of the coated beam pipe depends mostly on the coating thickness and not on the coating resistivity [7]. Unfortunately, it is often difficult to get reliable data on the physical properties of the coating layer, both thickness and resistivity, to estimate if this approximation holds. What is often done at this stage is to take a conservatively large value for the coating resistivity, as intuitively, a larger resistivity is expected to overestimate the impedance. But this intuitive consideration has been shown to be wrong [8] leading to false conclusions about the coating resistive-wall impedance and the real impact of the coating resistivity.

This paper starts by presenting different models for the two-layer circular beam pipe resistive-wall impedance in Sec. II to explain the effect of the coating resistivity on the impedance. Then, the example of SOLEIL II, a fourth generation light source in design [6,9], is used to show the impact of the coating resistivity on the microwave instability threshold in Sec. III. Finally, the findings are discussed in Sec. IV and conclusions are drawn in Sec. V.

II. ANALYTICAL ESTIMATION

Several models for the multilayer beam pipe have been developed over the years with different sets of approximations [10–12], but most of them end up in a complex formula from which it can be difficult to draw conclusions.

Among them, a simple enough formula for the two-layer circular beam pipe resistive-wall impedance has been expressed in practical form in [5]. The model used to derive the formula assumes a coating of thickness Δ and resistivity ρ_1 while the pipe is supposed infinitely thick with a resistivity ρ_2. For both materials, it is also assumed that $\rho\omega\epsilon \ll 1$, with ϵ the material permittivity, meaning the materials should be good enough conductors which is true for most of the materials used in accelerator beam pipes. The space charge effects are neglected, effectively expressing that it is the resistive-wall impedance and not the full "wall impedance":

$$\frac{Z_{\parallel}(\omega)}{C}=\frac{Z_0\omega}{4\pi cb}[\mathrm{sgn}(\omega)-i]\delta_1\frac{\alpha\tanh\left[\frac{1-i\mathrm{sgn}(\omega)}{\delta_1}\Delta\right]+1}{\alpha+\tanh\left[\frac{1-i\mathrm{sgn}(\omega)}{\delta_1}\Delta\right]}, \quad (1)$$

*alexis.gamelin@synchrotron-soleil.fr

$$\frac{Z_\perp(\omega)}{C} = \frac{Z_0}{2\pi b^3}[1 - i\mathrm{sgn}(\omega)]\delta_1 \frac{\alpha \tanh\left[\frac{1-i\mathrm{sgn}(\omega)}{\delta_1}\Delta\right] + 1}{\alpha + \tanh\left[\frac{1-i\mathrm{sgn}(\omega)}{\delta_1}\Delta\right]}, \tag{2}$$

where $Z_\parallel$ and $Z_\perp$ express, respectively, the longitudinal and transverse impedance at a given angular frequency ω, C is the machine circumference, Z_0 is the vacuum impedance, c is the speed of light in vacuum, b is the circular beam pipe radius, $\alpha \approx \delta_1/\delta_2$, δ_1 and δ_2 are, respectively, the skin depth of the coating and of the beam pipe material.

When there is no coating, i.e., $\Delta = 0$, these expressions are reduced to the usual thick resistive-wall formulas [13]:

$$\frac{Z_\parallel(\omega)}{C} = \frac{Z_0\omega\delta_2}{4\pi cb}[\mathrm{sgn}(\omega) - i] = \frac{\rho_2}{2\pi b\delta_2}[\mathrm{sgn}(\omega) - i] \tag{3}$$

$$\frac{Z_\perp(\omega)}{C} = \frac{Z_0\delta_2}{2\pi b^3}[1 - i\mathrm{sgn}(\omega)] = \frac{c\rho_2}{\omega\pi b^3\delta_2}[1 - i\mathrm{sgn}(\omega)]. \tag{4}$$

These expressions for the two-layer circular beam pipe resistive-wall impedance can be further simplified, as done in [5] if the assumption that the skin depth of the coating δ_1 is much larger than the coating thickness Δ is made:

$$\frac{Z_\parallel(\omega)}{C} \approx \frac{Z_0\omega}{4\pi cb}\left\{[\mathrm{sgn}(\omega) - i]\delta_2 - 2i\Delta\left(1 - \frac{\rho_2}{\rho_1}\right)\right\}, \tag{5}$$

$$\frac{Z_\perp(\omega)}{C} \approx \frac{Z_0}{2\pi b^3}\left\{[1 - i\mathrm{sgn}(\omega)]\delta_2 - 2i\Delta\mathrm{sgn}(\omega)\left(1 - \frac{\rho_2}{\rho_1}\right)\right\}, \tag{6}$$

In that case, it is clearly seen that the two-layer circular beam pipe resistive-wall impedance is composed of the usual thick wall impedance plus an inductive perturbation driven by the coating thickness Δ. In addition, if the coating resistivity ρ_1 is much larger than beam pipe resistivity ρ_2, then the inductive perturbation is reduced to $-\frac{iZ_0\omega\Delta}{2\pi cb}$ for the longitudinal impedance and to $-\frac{i\Delta\mathrm{sgn}(\omega)Z_0}{\pi b^3}$ for the transverse one. In both cases, the inductive perturbation is then independent of the coating resistivity ρ_1 and depends only on the coating thickness Δ.

The inductive behavior of the NEG coating has been observed experimentally [14,15] and the low sensitivity on the NEG resistivity under some conditions is well documented [5,7]. What might be less clear is the precise conditions under which it is possible to neglect the effect of the coating resistivity. From Eqs. (5) and (6), the condition is simply that $\rho_1 \gg \rho_2$ and is usually verified as beam pipe materials are chosen to be good conductors. But in order for Eqs. (5) and (6) to be valid, the condition $\delta_1 \gg \Delta$ is needed. The skin depth of the coating δ_1 is expressed as

$$\delta_1 = \sqrt{\frac{2\rho_1}{\omega\mu}}, \tag{7}$$

where μ is the coating magnetic permeability, for most coatings $\mu = \mu_r\mu_0 \approx \mu_0$. This condition can then be rewritten as a condition on the coating resistivity $\rho_1 \gg \frac{\omega\mu_0\Delta^2}{2} \approx \frac{\omega Z_0\Delta^2}{2c}$. Thus, the impedance of the two-layer circular beam pipe is independent of the coating resistivity ρ_1 at a given frequency ω only if

$$\rho_1 \gg \max\left(\rho_2, \frac{\omega Z_0\Delta^2}{2c}\right) \tag{8}$$

Figure 1 shows the validity domain of this approximation, using the arbitrary criteria that the coating resistivity should be 10 times greater than $\frac{\omega Z_0\Delta^2}{2c}$, as a function of the coating thickness Δ at different frequencies as solid lines. Measured resistivity values for different types of NEG are superimposed on the graph as dashed lines. The intersection between solid and dashed lines provides the approximate frequency and thickness after which the approximation breaks down and the NEG-coated beam pipe impedance will deviate from Eqs. (5) and (6).

In the study by Malyshev *et al.*, two NEG films composed of Ti-Zr-Hf-V are studied [8]. A resistivity of $\rho_{\mathrm{col}} = 7.1 \times 10^{-5}\ \Omega\,\mathrm{m}$ is measured for the columnar NEG at 7.8 GHz while the dense NEG film is measured at $\rho_{\mathrm{dense}} = 1.25 \times 10^{-6}\ \Omega\,\mathrm{m}$ [8]. The columnar NEG is produced using a dc deposition and is reported to have better

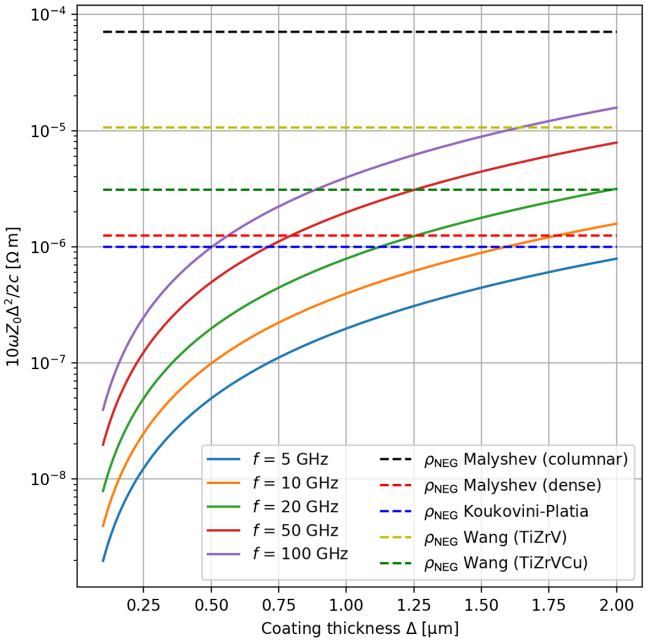

FIG. 1. Illustration of the validity domain of Eq. (8), corresponding to the region on the left side of each intersection between a solid and a dashed line.

pumping properties while the dense NEG is produced using high power impulse magnetron sputtering and is supposed to have lower photon and electron stimulated desorption. These two resistivity values will be used as examples in this article as the two corresponding NEG films are well characterized with different physical properties and resistivity. The study of Koukovini-Platia *et al.* reports a resistivity of 1×10^{-6} Ω m at 10 GHz for a Ti-Zr-V NEG film produced by magnetron sputtering [16]. Finally, the study of Wang *et al.* reports a resistivity of 1.07×10^{-5} Ω m for Ti-Zr-V and of 3.09×10^{-6} Ω m for Ti-Zr-V-Cu NEG films deposited via magnetron sputtering [17].

The spread of the measured values in the literature is not unexpected as the NEG film properties can change in an important way depending on the recipe used [8,17]. As shown in Fig. 1, the independence of the impedance on the NEG resistivity in the medium to high frequency region is only valid for very thin coatings or for the highest measured resistivities. For a standard $\Delta = 1$ μm coating with $\rho_{\mathrm{dense}} = 1.25 \times 10^{-6}$ Ω m, using the same criteria, the approximation is only valid up to 32 GHz.

Figure 2 shows the longitudinal and transverse resistive-wall impedance of a copper beam pipe coated with 1 μm of dense NEG on the left plot and of columnar NEG on the right plot. The expressions for the two-layer resistive-wall impedance are compared to the thick wall formula and to the exact solution computed using the ImpedanceWake2D (IW2D) code [18]. For the columnar NEG, the impedance is well described by Eqs. (5) and (6), and thus also by Eqs. (1) and (2) which are more general, and corresponds to the thick wall impedance plus an inductive perturbation. For the dense NEG, there are both inductive and resistive perturbations due to the coating compared to the thick wall impedance. The increase of the real part of the dense NEG-coated copper beam pipe amounts to a factor of 1.5 at 30 GHz and to more than a factor of 3 at 100 GHz.

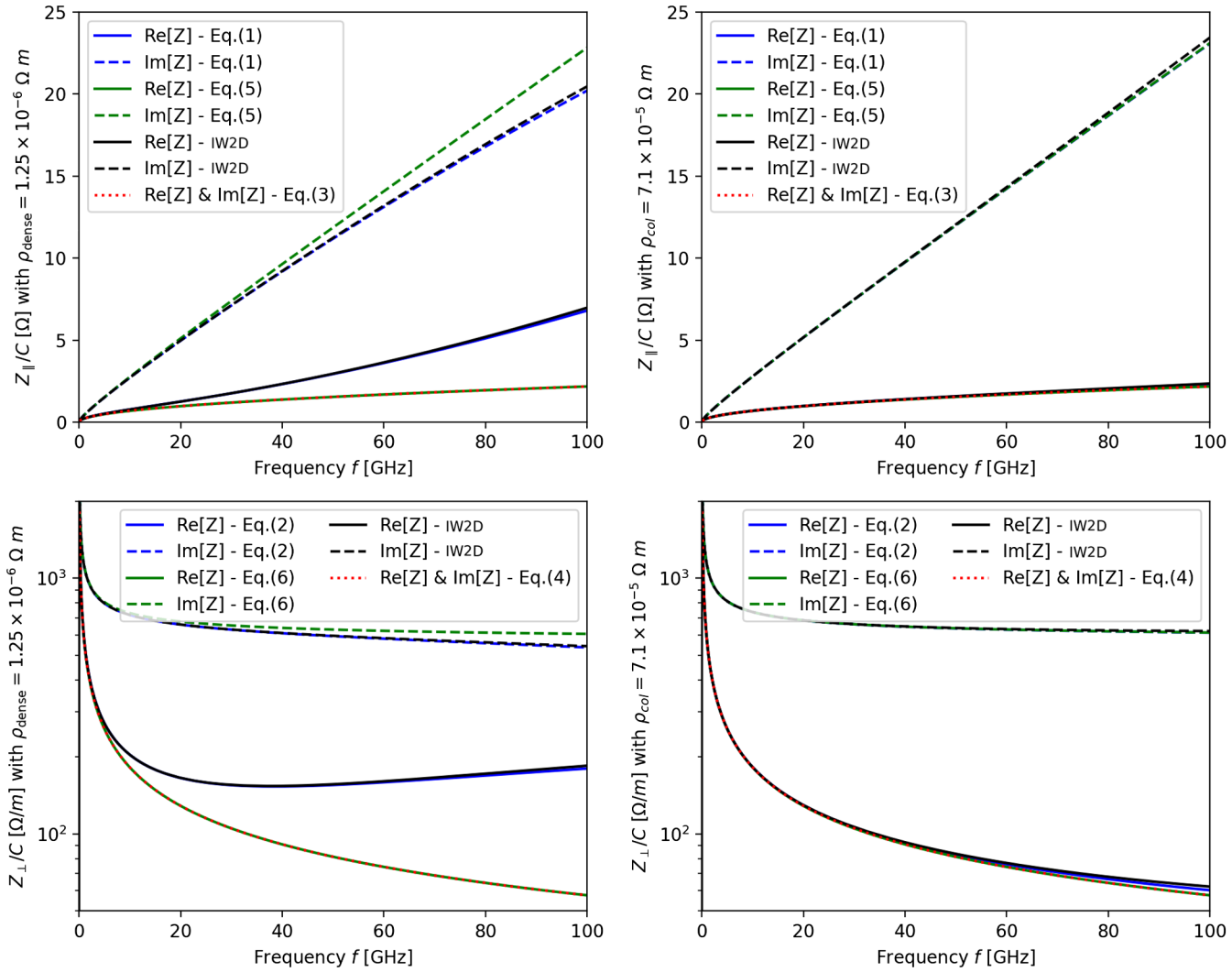

FIG. 2. Longitudinal (top) and transverse (bottom) resistive-wall impedance of a circular beam pipe coated with 1 μm of dense NEG (left) and columnar NEG (right). A beam pipe radius of 6 mm is used.

It means that a coating with a lower resistivity material can produce a higher (real part) impedance compared to a coating with higher resistivity material, this surprising result was pointed out in [8]. The physical explanation is that when the coating resistivity is high, the coating skin depth is large and thus the beam field can pass through the coating layer and enter the beam pipe layer which has a lower resistivity. On the contrary, when the coating resistivity is lower, the coating skin depth is also lower and the beam field is restricted to the coating layer which has still a lower conductivity than the beam pipe material.

Thus, during machine design, the idea of using a conservatively large value for the NEG resistivity with the aim of overestimating the impedance is incorrect and actually underestimates the impedance, potentially leading to misleading results [19,20]. In the same way, the approach taken in [17] to add copper to NEG film composition in order to reduce the wakefield strength is likely to produce results opposed to the initial goal.

The ratio of the loss factor with and without coating is shown in Fig. 3 for a $\sigma = 10$ ps Gaussian bunch versus the coating resistivity for different coating thickness Δ. It shows that the energy loss increase due to the coating is negligible for very thin coating or high resistivity coating but can be significant if the coating resistivity is low and the coating thickness is large. Of course, this effect highly depends on the beam frequency range and thus on the bunch length. For longer bunches, this effect is smaller: for a $\sigma = 30$ ps Gaussian bunch, the ratio of the loss factor is only $\frac{k_{\mathrm{loss,NEG}}}{k_{\mathrm{loss,RW}}} \approx 1.05$ for $\Delta = 1$ μm and $\rho_1 = 1 \times 10^{-6}$ Ω m compared to $\frac{k_{\mathrm{loss,NEG}}}{k_{\mathrm{loss,RW}}} \approx 1.19$ for a $\sigma = 10$ ps long bunch. For shorter bunches, it is stronger: $\frac{k_{\mathrm{loss,NEG}}}{k_{\mathrm{loss,RW}}} \approx 1.85$ for a $\sigma = 3$ ps long bunch in the same conditions.

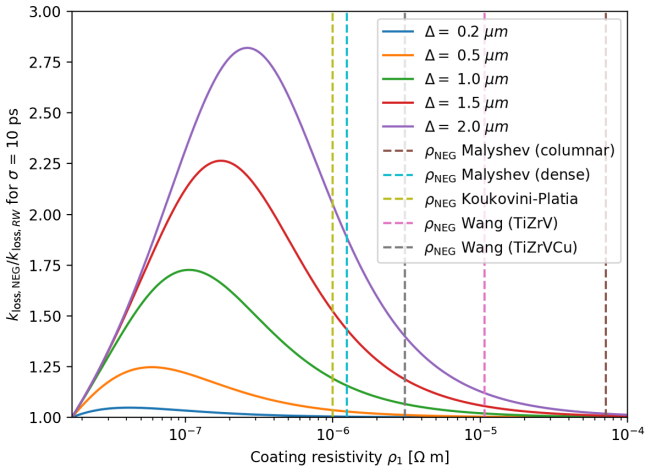

FIG. 3. Ratio of the NEG-coated copper beam pipe loss factor $k_{\mathrm{loss,NEG}}$ over the copper beam pipe loss factor $k_{\mathrm{loss,RW}}$ for a $\sigma = 10$ ps Gaussian bunch versus the NEG coating resistivity ρ_1 for different coating thickness Δ.

The resistivity of the beam pipe material ρ_2 is also an important parameter as the energy loss increase depends on the resistivity difference between the coating and the bulk material. For very good conductors like the copper beam pipe used in this study, the effect is the strongest, but for higher resistivity beam pipe materials, it is weaker as the coating and the bulk material are closer in value. For an aluminum beam pipe with $\Delta = 1$ μm, $\rho_1 = 1 \times 10^{-6}$ Ω m and $\sigma = 10$ ps, then $\frac{k_{\mathrm{loss,NEG}}}{k_{\mathrm{loss,RW}}} \approx 1.17$ while for a stainless steel beam pipe, it would be $\frac{k_{\mathrm{loss,NEG}}}{k_{\mathrm{loss,RW}}} \approx 1.02$.

Regarding the transverse plane, the kick factor computed from the two-layer beam pipe impedance is increased compared to a single-layer beam pipe but it is mostly independent of the coating resistivity as it depends only on the imaginary part of the impedance. As the kick factor is directly linked to the tune shift with current, one could expect the transverse mode-coupling instability (or head-tail instability) threshold to decrease for the two-layer beam pipe impedance. In fact, as shown in the next section, it is more of a competition between the increase of the kick factor and the increased bunch length, both effects being controlled by the coating thickness. For usual coating thickness, the real part of the impedance at very low frequencies is not affected by coatings so, at first order (neglecting the bunch length change which can affect the head-tail damping), the multibunch resistive-wall instability should not be impacted by coatings.

As the increase of the real part of the two-layer circular beam pipe resistive-wall impedance is important at high frequencies, this effect is important for storage rings or linacs aiming for short bunches. Most fourth-generation light sources built or in design are aiming for rather long bunches using harmonic cavities, so one could think that the impact of this effect is limited. But, as it will be shown in the next section, this effect can still impact the threshold of the microwave instability (MWI) even when the bunch length is quite large.

III. TRACKING

In this section, the consequences of the high frequency increase of the real part of the NEG coated beam pipe resistive-wall impedance are investigated by tracking simulations in the framework of the SOLEIL II project.

The SOLEIL II project aims to upgrade the SOLEIL storage ring, the French third-generation light source [21], to a fourth-generation light source [6,9,22]. The storage ring lattice parameters used for this study are reported in Table I.

The tracking study is done using MBTRACK2, an open-source collective effect library written in python3 [23,24]. The tracking part of MBTRACK2 is designed to be able to integrate both single and multi-bunch collective effects. Here the single bunch effects of the NEG-coated beam pipe are introduced by using the WakePotential class. This class

TABLE I. Parameters used for tracking for SOLEIL II storage ring.

Parameter	Value
Electron beam energy	2.75 GeV
Natural emittance	80 pm
Circumference	354.7 m
Harmonic number	416
Momentum compaction factor	9.12×10^{-5}
Energy loss per turn	515 keV
Longitudinal damping time	11.7 ms
Relative energy spread	9×10^{-4}
Main rf voltage	1.7 MV
Natural bunch length	8.2 ps

can compute a wake potential from any uniformly sampled wake function. First, the bunch macroparticles are sorted longitudinally into bins using a variable grid to compute the bunch charge density profile and its dipole moment. Then the bunch profile is interpolated on the wake function time base which is used to perform the convolution to get the wake potential.

To make sure that the observed effect comes only from the coated beam pipe, the impedance model considered is kept very simple on purpose: a uniform copper beam pipe of 6 mm radius for the full ring circumference. Three scenarios are studied: the beam pipe is coated with columnar NEG ($\rho_{\mathrm{col}} = 7.1 \times 10^{-5}\,\Omega\mathrm{m}$), the beam pipe is coated with dense NEG ($\rho_{\mathrm{dense}} = 1.25 \times 10^{-6}\ \Omega\,\mathrm{m}$), the beam pipe is not coated (corresponding to pure copper resistive-wall impedance). The coating thickness Δ is varied from 0.5 μm to 1.5 μm in order to understand its impact.

The wake functions $W_{\parallel}$ used for tracking are computed using IW2D [18] and are shown in Fig. 4 for a coating thickness of $\Delta = 1$ μm and a length of 1 m. Those wake functions are computed for SOLEIL II energy so they do not respect the "causality principle" which states that $W_{\parallel}(t < 0) = 0$ as it is only strictly valid for $v = c$. A wake function computed for $\gamma \approx \infty$ is shown to highlight the (small) difference around $t \approx 0$.

One can see that the columnar NEG wake function shows a strong ringing compared to the dense NEG and the copper-only wake functions. It can be explained by its much more peaked impedance at very high frequency as shown in Fig. 5. The coating resistivity impacts not only the broadband part of the resistive-wall impedance but also its peak frequency and quality factor. If the coating resistivity ρ_1 is close to one of its substrate ρ_2, then the peak frequency and quality factor are close to the substrate-only impedance. When the coating resistivity ρ_1 is larger, the peak frequency is shifted downward and the quality factor increases.

The wake potentials from MBTRACK2 and from analytical computations are shown in Fig. 6 for a Gaussian bunch of $\sigma = 8.2$ ps. The main difference between the two methods is that the analytic method assumes a perfect Gaussian bunch distribution while the MBTRACK2 uses the tracking algorithm. Here the tracked bunch is composed of $N_{mp} = 4 \times 10^6$ macroparticles, initialized to have a Gaussian distribution, and sorted in $N_{\mathrm{bin}} = 100$ bins. It can be seen that there is good agreement between both methods in all cases but that NEG wake potentials are a bit noisier than the pure copper wake. The reason is the very inductive nature of the NEG impedance compared to the standard resistive-wall impedance, it makes the wake potential sensible to the derivative of the bunch profile and thus more sensitive to numerical noise. Another way to check the numerically computed wake potentials is to compare the time domain (TD) loss factor k_{loss} computed using this wake potential

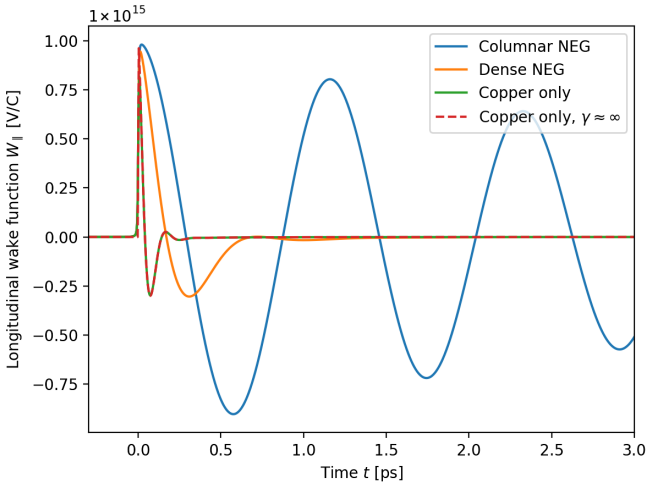

FIG. 4. Longitudinal wake functions $W_{\parallel}$ for the columnar NEG, dense NEG, and copper (with finite γ and $\gamma \approx \infty$). The coating thickness used is $\Delta = 1$ μm.

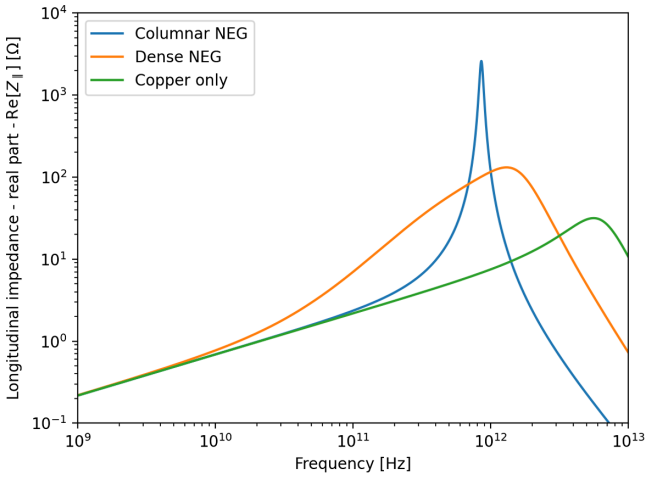

FIG. 5. Real part of the longitudinal impedance Re$[Z_{\parallel}]$ for the columnar NEG, dense NEG, and copper computed using IW2D [18]. The coating thickness used is $\Delta = 1$ μm.

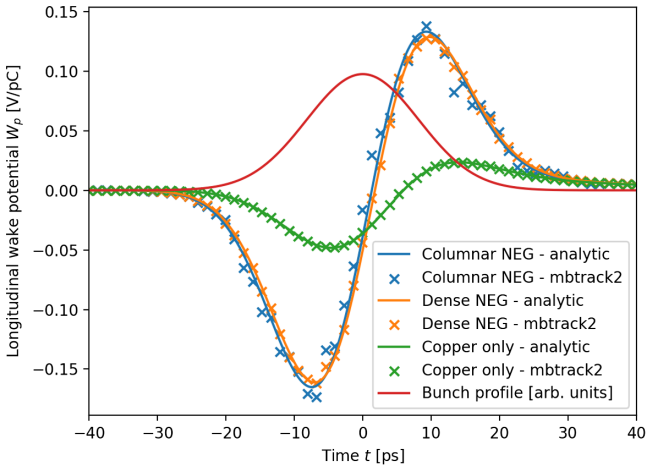

FIG. 6. Longitudinal wake potential W_p for the columnar NEG, dense NEG, and copper from analytical computation and from MBTRACK2. The coating thickness used is $\Delta = 1$ μm.

against the loss factor computed in the frequency domain (FD) using the impedance with a perfect Gaussian distribution as done in Table II.

The tracking results are shown in Fig. 7 for a coating thickness Δ varying from 0.5 to 1.5 μm. The bunch length σ_s versus the single bunch current I is shown on the left plots while the relative energy spread $\sigma_\delta/\sigma_{\delta,0}$ increase is shown on the right plots. The single bunch current I is varied from 0 to 20 mA and each current point corresponds to different tracking simulations for 60×10^3 turns (to be compared with a longitudinal damping time close to 10×10^3 turns). Then the mean value of the bunch length σ_s and relative energy spread $\sigma_\delta/\sigma_{\delta,0}$ are computed on the last 10×10^3 turns and their standard deviation are used as error bars.

As expected, the main effect of both types of NEG is to increase the bunch lengthening with current. With copper chamber without NEG, the bunch length increases from the zero current value of 8.2 to 19 ps at 20 mA. Whereas with a 0.5 μm thick NEG coating it is 23 ps at 20 mA, this value increases close to 30 ps for a μm thick coating.

What is more surprising is the increase of the relative energy spread $\sigma_\delta/\sigma_{\delta,0}$ observed, characteristic of the microwave instability (MWI). No energy spread increase is observed when only the copper chamber without coating is taken into account, suggesting that the MWI threshold is higher than the maximum single bunch current of 20 mA used for this study. A MWI threshold, corresponding to the first increase of energy spread from its nominal value $\sigma_{\delta,0}$, is observed for both columnar and dense NEG cases. For the dense NEG, the MWI threshold decreases when the coating thickness Δ increases but the behavior is quite different for the columnar NEG. The reason is that the main effect of coating thickness increase is to lengthen more the bunches, which in turn changes the overlap between the bunch frequency spectrum and the longitudinal impedance. The columnar NEG impedance is sharply peaked at high frequency while the dense NEG is more broadband (see Fig. 5), so the MWI threshold for the columnar NEG will be triggered when the bunch length σ_s is shorter corresponding to a higher overlap with the high frequency region while the dense NEG MWI threshold is triggered by the increasing magnitude of the longitudinal impedance when the coating thickness Δ is increased (see Fig. 3).

This effect is clearly visible for $\Delta = 0.5$ μm, the bunch lengthening due to NEG is small so the columnar MWI threshold is around 10 mA while the dense one is around 18 mA. For the simulation from $\Delta = 0.75$–1.25 μm, the bunch lengthening due to NEG increases, and the columnar MWI threshold and dense MWI threshold go in opposite directions. For $\Delta = 1.5$ μm, the columnar MWI threshold rises from a very low current (when the bunch length is short), but the energy spread decreases at higher currents because the bunch length increases. The slightly different behavior observed for $\Delta = 1.5$ μm (and also a bit for $\Delta = 1.25$ μm) is linked to the downward frequency shift of the columnar resonance when Δ increases. The resonance of the columnar NEG shown in Fig. 5 is around 855 GHz for $\Delta = 1.0$ μm but is shifted to 700 GHz for $\Delta = 1.5$ μm, and to 1.2 THz for $\Delta = 0.5$ μm.

As this kind of macroparticle tracking simulation is very sensitive to numerical noise, a convergence study has been conducted to check these results which details are presented in Appendix A. Further checks are presented in Appendix B where the same simulations are ran using a totally different method consisting of solving numerically the Vlasov-Fokker-Plank equation using the INOVESA code [25].

Apart from the longitudinal beam dynamics, the effect of NEG coating on the transverse one was also investigated by tracking. The study focused on the head-tail instability at the nominal chromaticity of 1.6 and a NEG coating thickness of $\Delta = 1.0$ μm. The results showed that the head-tail instability was actually efficiently suppressed with NEG coating (both types) within a range from 0 to 20 mA, compared to an uncoated copper pipe for which the current threshold was found around 13 mA. This is in contradiction with the expectation that the head-tail instability growth rate should increase in the NEG-coated case because of the added inductive perturbation seen in Fig. 2.

TABLE II. Loss factor k_{loss} computed in time domain (TD) from tracking and in frequency domain (FD) assuming a perfect Gaussian distribution.

	TD (V pC^{-1})	FD (V pC^{-1})	Relative error (%)
Columnar NEG	0.0228	0.0229	−0.536
Dense NEG	0.0273	0.0274	−0.532
Copper	0.0227	0.0229	−0.548

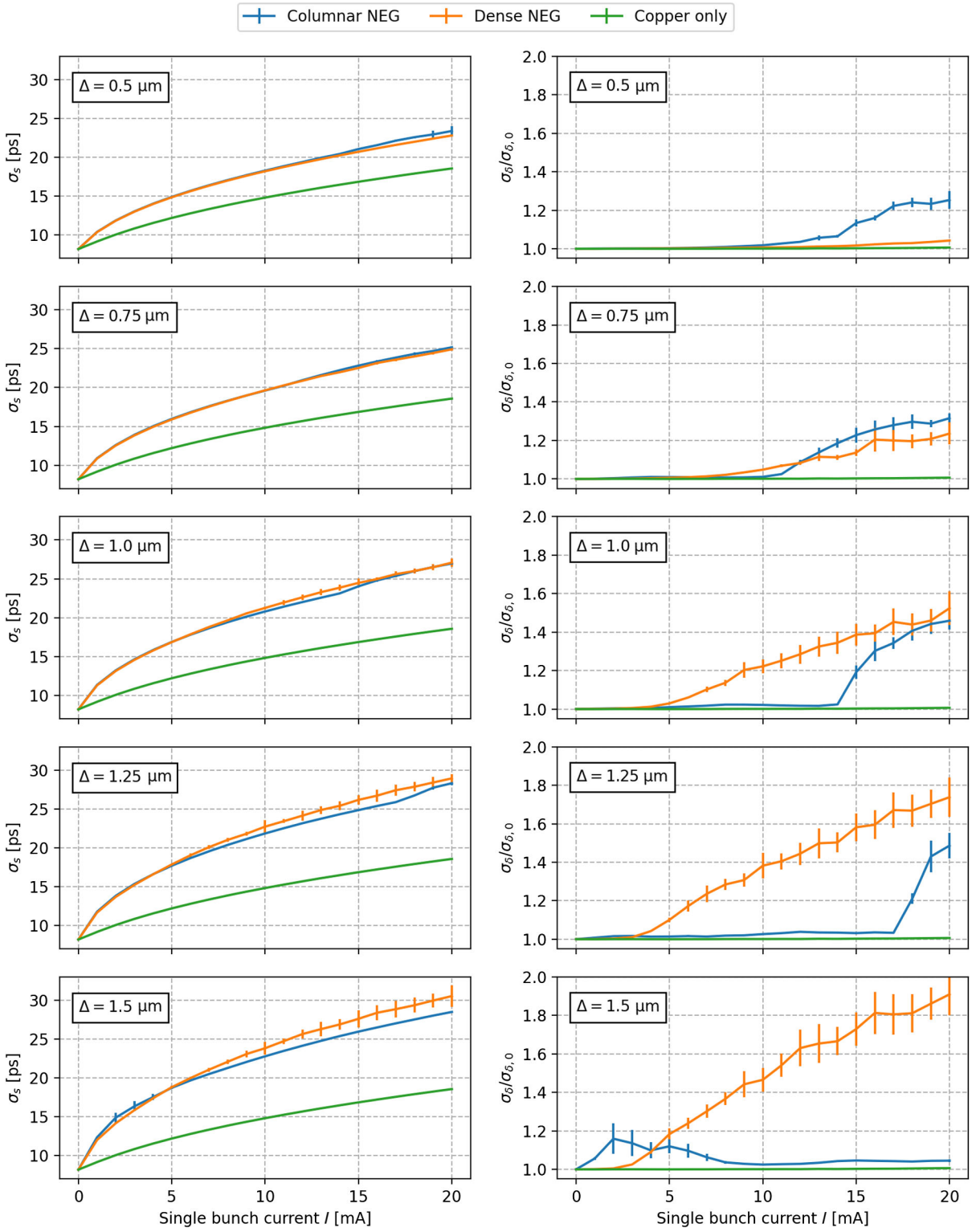

FIG. 7. Bunch length σ_s (on the left) and relative energy spread $\sigma_\delta/\sigma_{\delta,0}$ (on the right) versus single bunch current I from tracking for different NEG coating thickness Δ.

This result can be explained by the strong bunch lengthening induced by the NEG coating. To confirm this hypothesis, the tracking was also done without taking into account the longitudinal impedance, in that case, the threshold for both columnar and dense NEG is found near 4 mA. The conclusion on the increased head-tail threshold may differ for a different coating thickness but it shows that both NEG types behave similarly.

IV. DISCUSSION

The significance of these results largely depends on the application case. As it has been explained in Sec. II, the influence of the NEG resistivity is stronger at high frequencies so a more important effect is expected for shorter bunches. But even when the bunch length gets longer because of the NEG inductive behavior or due to harmonic cavities, the NEG resistivity can strongly impact the MWI threshold as shown in Sec. III. For a commonly used NEG thickness like 1 μm, there is a factor of 3 on the MWI threshold variation between different NEG resistivities in the SOLEIL II case. Of course, this is to be compared with the MWI threshold from other impedance sources like the broadband impedance and the coherent synchrotron radiation impedance. But this effect could potentially explain part of the discrepancy observed between measurements and prediction based on impedance models [26]. Especially, when a conservatively large value is taken for the NEG resistivity leading to possibly artificially higher thresholds.

As stated before, this effect also depends on the beam pipe resistivity and is expected to be at its strongest for copper. It should be checked for aluminum chambers but is probably negligible for stainless steel chambers.

Regarding the NEG resistivity, as already discussed in Sec. II, its value is likely strongly linked to the recipe used and the deposition method. Different measurements made on CERN-made samples give a value in the order of 1×10^{-6} Ω m [16,27,28], which seems to indicate that this value is consistent for this particular recipe. NEG made with other recipes or deposition methods, from private companies or other labs, may give different resistivity when it is measured [8,17] but in most cases, it is an unknown quantity.

If the beam pipe dimensions are much larger in one direction compared to the other, the NEG coating thickness can be reduced where the surface is close to the beam path while leaving a larger thickness elsewhere where the image current is not flowing as it has been done in SOLEIL. If it is not possible, most probably, the best solution is to reduce the NEG layer thickness as much as possible in order not to be sensitive to the NEG resistivity which might not be a fully known parameter. This approach is the one followed in the FCC-ee studies where the coating proposed is in the 50 to 100 nm range [5,29]. But realizing such thin NEG coating in small chambers while ensuring that the vital pumping properties of the NEG are preserved is difficult and is probably out of reach for most accelerator labs. Also, the reduction of the NEG film thickness has been shown to impact the NEG pumping properties [30].

In addition, past measurements of the NEG thickness deposited in small aperture vacuum chamber (from 6 to 10 mm diameter) have shown a longitudinal variation of 40% of the NEG thickness compared to the mean thickness value measured [31]. This kind of thickness spread can lead to a different impedance compared to the impedance of a pipe coated with the mean thickness value. It could also have the effect of spreading out in frequency domain a columnar NEG-like resonance which depends on the thickness Δ. The contribution of the surface roughness impedance due to the longitudinal variation of the NEG coating is also to consider [32].

For SOLEIL II project, this study has led to reduce the NEG coating thickness target from 1 μm down to 0.5 μm in order to reduce the NEG impedance and the uncertainty due to the mostly unknown coating resistivity. The value of the MWI threshold simulated with dense NEG for $\Delta = 1$ μm is about 4 mA, which is close to the MWI threshold obtained with the full impedance model of the conceptual design report, $I_{\mathrm{th}} \approx 2.5 \pm 1$ mA [6,19]. With a coating around 0.5 μm, more margin is expected with respect to the MWI threshold driven by other impedance types.

V. CONCLUSIONS

The influence of the coating resistivity on the two-layer beam pipe resistive-wall impedance and on beam dynamics has been thoroughly investigated. In order to make the conclusions more general, the effect of most of the other relevant parameters such as the coating thickness, bunch length, etc. was also explored. However, it should be emphasized that the conclusions presented in this section are based solely on the example of SOLEIL II and may vary for other machines depending on their specific parameters. It is found that (i) a coating with a lower resistivity material can produce an impedance with a higher real part compared to a coating with higher resistivity material, as pointed out in [8]; (ii) the resistivity value of a coating can strongly impact the microwave instability threshold and the consequent energy spread increase; (iii) the overestimation of the coating resistivity can lead to an overestimation of the real microwave instability threshold; (iv) reducing the coating thickness helps to be less sensitive to the coating resistivity.

ACKNOWLEDGMENTS

The authors would like to thank Miriam Brosi for her help in getting started with INOVESA simulations. The authors also thank SOLEIL vacuum and accelerator physics groups for their support and discussions. Part of this work was carried out as part of the second author's Ph.D. funded by the French Embassy's Franco-Thai Scholarship Program.

APPENDIX A: CONVERGENCE STUDY

As MWI simulations are quite sensitive to numerical noise, different tracking parameters have been varied to make sure that the tracking results are accurate. A convergence study has been done by varying the macroparticle number N_{mp} from 1×10^6 to at least 4×10^6 for all the simulated cases presented in this article. The case

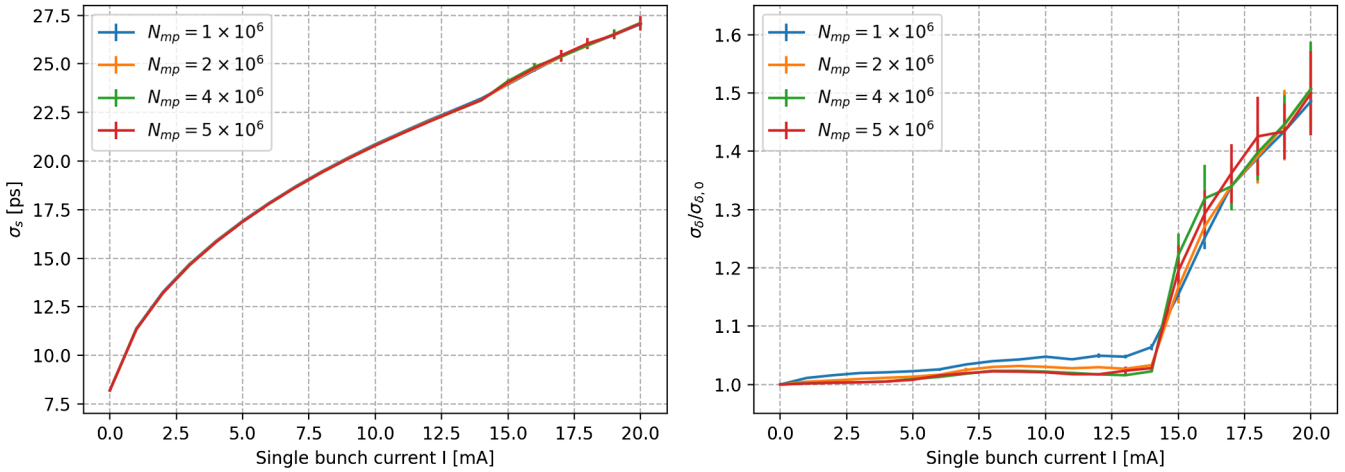

FIG. 8. Tracking results using different macroparticle number N_{mp}. Bunch length σ_s is shown on the left plot and relative energy spread $\sigma_\delta/\sigma_{\delta,0}$ on the right plot versus single bunch current I. Case corresponding to columnar NEG with $\Delta = 1$ μm.

corresponding to columnar NEG with a thickness $\Delta = 1$ μm is shown in Fig. 8 for N_{mp} up to 5×10^6. There is no significant variation of the bunch length σ_s and small variation of the relative energy spread $\sigma_\delta/\sigma_{\delta,0}$ between $N_{mp} = 1 \times 10^6$ and $N_{mp} = 2 \times 10^6$. It indicates that the tracking results are fully converged from $N_{mp} = 2 \times 10^6$, this is also the case for all simulated cases. The sampling of the input wake functions and the bin number N_{bin} were also varied on some specific cases to make sure that they had no influence on the tracking results.

APPENDIX B: BENCHMARK WITH VLASOV-FOKKER-PLANCK SOLVER INOVESA

INOVESA is a code that solves the Vlasov-Fokker-Plank equation on a grid [25,33]. It has mainly been used to study the MWI induced by coherent synchrotron radiation and has been successfully benchmarked against theory and experiment [25,34,35]. Here, this code is used to provide a totally different way of exploring this problem, as not only the method is different but also the input since INOVESA computes the wake force in the frequency space so using the impedance and not the wake function. The impedances used as input for the code were computed using IW2D and are the ones shown in Fig. 5.

Figure 9 shows the simulation results obtained with MBTRACK2 and INOVESA for the copper resistive-wall impedance and for the impedance of the copper chamber coated with a 1-μm dense NEG film. INOVESA simulations were straightforward enough for the copper resistive-wall impedance as a good result was obtained using numerical parameters close to the default ones. It was not the case when the NEG impedance was used as input, probably because of the much more inductive nature of its impedance compared to the copper resistive impedance. After tweaking the numerical parameters of the code, i.e., increasing

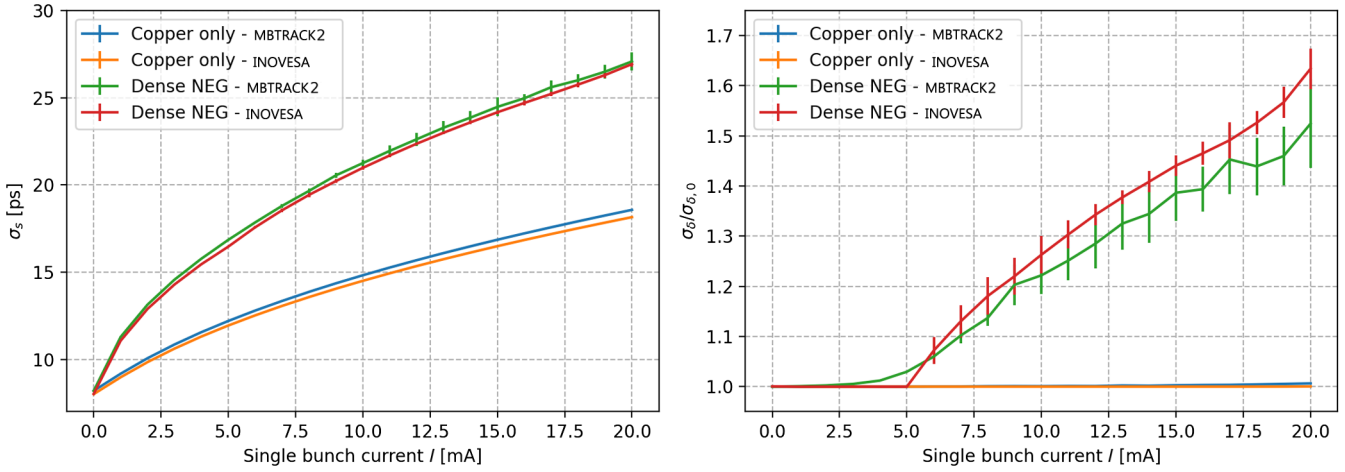

FIG. 9. Simulations results with MBTRACK2 and INOVESA. Bunch length σ_s is shown on the left plot and relative energy spread $\sigma_\delta/\sigma_{\delta,0}$ on the right plot versus single bunch current I. Case corresponding to dense NEG is with $\Delta = 1$ μm.

the phase space size, grid size, and number of steps per synchrotron period, it was possible to get a convergence for the dense NEG impedance. Unfortunately, we did not succeed in finding the same convergence for the columnar NEG impedance case because of a numerical instability leading to a triangular bunch shape. A possible reason for this numerical instability would be the strong oscillatory nature of the columnar NEG at high frequencies.

[1] C. Benvenuti, P. Chiggiato, F. Cicoira, and Y. L'Aminot, Nonevaporable getter films for ultrahigh vacuum applications, J. Vac. Sci. Technol. A **16**, 148 (1998).

[2] C. Benvenuti, J. M. Cazeneuve, P. Chiggiato, F. Cicoira, A. E. Santana, V. Johanek, V. Ruzinov, and J. Fraxedas, A novel route to extreme vacua: The non-evaporable getter thin film coatings, Vacuum **53**, 219 (1999).

[3] C. Benvenuti, P. Chiggiato, P. C. Pinto, A. E. Santana, T. Hedley, A. Mongelluzzo, V. Ruzinov, and I. Wevers, Vacuum properties of TiZrV non-evaporable getter films, Vacuum **60**, 57 (2001).

[4] E. Belli, M. Migliorati, B. Spataro, S. Persichelli, A. Novokhatski, G. Castorina, and M. Zobov, Coupling impedances and collective effects for FCC-ee, in *Proceedings of the 8th International Particle Accelerator Conference, IPAC-2017, Copenhagen, Denmark* (JACoW, Geneva, Switzerland, 2017), Vol. 17.

[5] M. Migliorati, E. Belli, and M. Zobov, Impact of the resistive wall impedance on beam dynamics in the Future Circular e^+e^- Collider, Phys. Rev. Accel. Beams **21**, 041001 (2018).

[6] Conceptual design report Synchrotron SOLEIL upgrade, Synchrotron SOLEIL, Technical Report, 2021.

[7] R. Nagaoka, Study of resistive-wall effects on SOLEIL, in *Proceedings of the 9th European Particle Accelerator Conference, Lucerne, 2004* (EPS-AG, Lucerne, 2004).

[8] O. B. Malyshev, L. Gurran, P. Goudket, K. Marinov, S. Wilde, R. Valizadeh, and G. Burt, RF surface resistance study of non-evaporable getter coatings, Nucl. Instrum. Methods Phys. Res., Sect. A **844**, 99 (2017).

[9] A. Loulergue, D. Amorim, O. Blanco-García, P. Brunelle, W. Foosang, A. Gamelin, A. Nadji, L. Nadolski, R. Nagaoka, R. Ollier, and M.-A. Tordeux, TDR baseline lattice for the upgrade of SOLEIL, in *Proceedings of the 13th International Particle Accelerator Conference, IPAC-2022, Bangkok, Thailand* (JACoW, Geneva, Switzerland, 2022).

[10] N. Wang and Q. Qin, Resistive-wall impedance of two-layer tube, Phys. Rev. ST Accel. Beams **10**, 111003 (2007).

[11] Y. Shobuda and Y. H. Chin, Resistive-wall impedances of a thin non-evaporable getter coating on a conductive chamber, Prog. Theor. Exp. Phys. **2017**, 123G01 (2017).

[12] N. Mounet and E. Métral, Electromagnetic field created by a macroparticle in an infinitely long and axisymmetric multilayer beam pipe, CERN Technical Report No. CERN-BE-2009-039, 2009.

[13] A. Chao, *Physics of Collective Beam Instabilities in High Energy Accelerators* (Wiley, New York, 1993).

[14] E. Karantzoulis, V. Smaluk, and L. Tosi, Broad band impedance measurements on the electron storage ring ELETTRA, Phys. Rev. ST Accel. Beams **6**, 030703 (2003).

[15] P. Brunelle, R. Nagaoka, and R. Sreedharan, Measurement and analysis of the impact of transverse incoherent wake-fields in a light source storage ring, Phys. Rev. Accel. Beams **19**, 044401 (2016).

[16] E. Koukovini-Platia, G. Rumolo, and C. Zannini, High frequency electromagnetic characterization of NEG properties for the CLIC damping rings, in *Proceedings of the 5th International Particle Accelerator Conference, IPAC-2014, Dresden, Germany* (JACoW, Geneva, Switzerland, 2014).

[17] S. Wang, B. Zhu, Y. Gao, X. Shu, W. Wei, W. Zhang, and Y. Wang, On the synergy manipulation between the activation temperature, surface resistance and secondary electron yield of NEG thin films, Appl. Surf. Sci. **578**, 152101 (2022).

[18] N. Mounet, ImpedanceWake2D, https://gitlab.cern.ch/IRIS/IW2D.

[19] A. Gamelin, D. Amorim, P. Brunelle, W. Foosang, A. Loulergue, L. Nadolski, R. Nagaoka, R. Ollier, and M.-A. Tordeux, Collective effects studies for the SOLEIL upgrade, in *Proceedings of the 12th International Particle Accelerator Conference, IPAC-2021, Campinas, SP, Brazil* (JACoW, Geneva, Switzerland, 2021).

[20] M. Abbott *et al.*, Diamond-II technical design report, Diamond Light Source, Technical Report, 2022.

[21] L. Nadolski *et al.*, in *Proceedings of the 13th International Particle Accelerator Conference, IPAC-2022, Bangkok, Thailand* (JACoW, Geneva, Switzerland, 2022).

[22] A. Nadji and L. S. Nadolski, Upgrade project of the SOLEIL Accelerator Complex, Synchrotron Radiat. News **36**, 10 (2023).

[23] A. Gamelin, W. Foosang, and R. Nagaoka, MBTRACK2, a collective effect library in Python, in *Proceedings of the 12th International Particle Accelerator Conference, IPAC-2021, Campinas, SP, Brazil* (JACoW, Geneva, Switzerland, 2021).

[24] A. Gamelin, MBTRACK2, https://gitlab.synchrotron-soleil.fr/PA/collective-effects/mbtrack2.

[25] P. Schönfeldt, M. Brosi, M. Schwarz, J. L. Steinmann, and A.-S. Müller, Parallelized Vlasov-Fokker-Planck solver for desktop personal computers, Phys. Rev. Accel. Beams **20**, 030704 (2017).

[26] V. Smaluk, Impedance computations and beam-based measurements: A problem of discrepancy, Nucl. Instrum. Methods Phys. Res., Sect. A **888**, 22 (2018).

[27] A. Passarelli, H. Bartosik, G. Rumolo, V. G. Vaccaro, M. R. Masullo, C. Koral, G. P. Papari, A. Andreone, and O. Boine-Frankenheim, Novel measurement technique for the electromagnetic characterization of coating materials in the sub-THz frequency range, Phys. Rev. Accel. Beams **21**, 103101 (2018).

[28] A. Passarelli, C. Koral, M. R. Masullo, W. Vollenberg, L. L. Amador, and A. Andreone, Sub-THz waveguide spectroscopy of coating materials for particle accelerators, Condens. Matter Theories **5**, 9 (2020).

[29] E. Belli, P. C. Pinto, G. Rumolo, A. Sapountzis, T. Sinkovits, M. Taborelli, B. Spataro, M. Zobov,

G. Castorina, and M. Migliorati, Electron cloud buildup and impedance effects on beam dynamics in the Future Circular e+e- Collider and experimental characterization of thin TiZrV vacuum chamber coatings, Phys. Rev. Accel. Beams **21**, 111002 (2018).

[30] Y. Gao, O. B. Malyshev, R. Valizadeh, Y. Hu, A. Hannah, J. Wang, J. Zhang, Y. Xie, Q. Sun, Z. You, Q. Si, and S. Wang, Effect of the film thickness on pumping properties of Ti–Zr–V coating, Nucl. Instrum. Methods Phys. Res., Sect. A: **1029**, 166474 (2022).

[31] P. Porcelli, NEG coating deposition of small-gap chambers: An industrial point of view, in *Proceedings of the 8th Low Emittance Ring Workshop, Frascati, INFN-LNF, Italy* (2020), https://agenda.infn.it/event/20813/contributions/122394/attachments/76561/98464/SAES_Presentation_LER_Workshop_28102020.pdf.

[32] G. Stupakov, Surface roughness impedance, AIP Conf. Proc. **581**, 141 (2001).

[33] P. Schönfeldt, Inovesa, https://github.com/Inovesa/Inovesa.

[34] J. L. Steinmann, T. Boltz, M. Brosi, E. Bründermann, M. Caselle, B. Kehrer, L. Rota, P. Schönfeldt, M. Schuh, M. Siegel, M. Weber, and A.-S. Müller, Continuous bunch-by-bunch spectroscopic investigation of the microbunching instability, Phys. Rev. Accel. Beams **21**, 110705 (2018).

[35] M. Brosi, S. Bielawski, C. Evain, A.-S. Müller, E. Roussel, P. Schreiber, and C. Szwaj, Simulations of the micro-bunching instability for SOLEIL and KARA using two different VFP solver codes, in *Proceedings of the 13th International Particle Accelerator Conference, Bangkok, Thailand* (JACoW, Geneva, Switzerland, 2022), pp. 2237–2240.